Original Article

Optimization of imaging parameters in chest CT for COVID-19 patients: an experimental phantom study

Yantao Niu[1], Shunxing Huang[2], Huan Zhang[2], Shuo Li[2], Xiaoting Li[3], Zhibin Lv[2], Shuo Yan[2], Wei Fan[4], Yanlong Zhai[5], Eddy Wong[6], Kexin Wang[2], Zongrui Zhang[1], Budong Chen[2], Ruming Xie[2], Junfang Xian[1]

[1]Department of Radiology, Beijing Tongren Hospital, Capital Medical University, Beijing, China; [2]Department of Radiology, Beijing Ditan Hospital, Capital Medical University, Beijing, China; [3]Department of Radiology, Peking University Cancer Hospital and Institute, Key Laboratory of Carcinogenesis and Translational Research (Ministry of Education/Beijing), Beijing, China; [4]Department of Radiology, Beijing Shijitan Hospital, Capital Medical University, Beijing, China; [5]Department of Cardiology, Beijing Tsinghua Changgung Hospital, School of Clinical Medicine, Tsinghua University, Beijing, China; [6]Philips CT Global Clinical Science, Philips Healthcare, Cleveland, OH, USA

Correspondence to: Junfang Xian. Department of Radiology, Beijing Tongren Hospital, Capital Medical University, No.1 Dongjiaominxiang Dongcheng District, Beijing 100730, China. Email: cjr.xianjunfang@vip.163.com; Ruming Xie. Department of Radiology, Beijing Ditan Hospital, Capital Medical University, No.8 Jingshun East Street, Chaoyang District, Beijing 100015, China. Email: 13911320739@163.com.

Background: With the global outbreak of coronavirus disease 2019 (COVID-19), chest computed tomography (CT) is vital for diagnosis and follow-up. The increasing contribution of CT to the population-collected dose has become a topic of interest. Radiation dose optimization for chest CT of COVID-19 patients is of importance in clinical practice. The present study aimed to investigate the factors affecting the detection of ground-glass nodules and exudative lesions in chest CT among COVID-19 patients and to find an appropriate combination of imaging parameters that optimize detection while effectively reducing the radiation dose.

Methods: The anthropomorphic thorax phantom, with 9 spherical nodules of different diameters and CT values of −800, −630, and 100 HU, was used to simulate the lesions of COVID-19 patients. Four custom-simulated lesions of porcine fat and ethanol were also scanned at 3 tube potentials (120, 100, and 80 kV) and corresponding milliampere-seconds (mAs) (ranging from 10 to 100). Separate scans were performed at pitches of 0.6, 0.8, 1.0, 1.15, and 1.49, and at collimations of 10, 20, 40, and 80 mm at 80 kV and 100 mAs. CT values and standard deviations of simulated nodules and lesions were measured, and radiation dose quantity (volume CT dose index; CTDIvol) was collected. Contrast-to-noise ratio (CNR) and figure of merit (FOM) were calculated. All images were subjectively evaluated by 2 radiologists to determine whether the nodules were detectable and if the overall image quality met diagnostic requirements.

Results: All simulated lesions, except −800 HU nodules, were detected at all scanning conditions. At a fixed voltage of 120 or 100 kV, with increasing mAs, image noise tended to decrease, and the CNR tended to increase ($F=9.694$ and $P=0.033$ for 120 kV; $F=9.028$ and $P=0.034$ for 100 kV). The FOM trend was the same as that of CNR ($F=2.768$ and $P=0.174$ for 120 kV; $F=1.915$ and $P=0.255$ for 100 kV). At 80 kV, the CNRs and FOMs had no significant change with increasing mAs ($F=4.522$ and $P=0.114$ for CNRs; $F=1.212$ and $P=0.351$ for FOMs). For the 4 nodules of −800 and −630 HU, CNRs had no statistical differences at each of the 5 pitches ($F=0.673$, $P=0.476$). The CNRs and FOMs at each of the 4 collimations had no statistical differences ($F=2.509$ and $P=0.125$ for CNRs; $F=1.485$ and $P=0.309$ for FOMs) for each nodule. CNRs and subjective evaluation scores increased with increasing parameter values for each imaging iteration. The CNRs of 4 −800 HU nodules in the qualified images at the thresholds of scanning parameters of 120 kV/20 mAs, 100 kV/40 mAs, and 80 kV/80 mAs, had statistical differences ($P=0.038$), but the FOMs had no statistical differences ($P=0.085$). Under the 3 threshold conditions, the CNRs and FOMs of the 4 nodules were highest at 100 kV and 40 mAs (1.6 mGy CTDIvol).

Conclusions: For chest CT among COVID-19 patients, it is recommended that 100 kV/40 mAs is used for average patients; the radiation dose can be reduced to 1.6 mGy with qualified images to detect ground-glass nodules and exudation lesions.

Keywords: Coronavirus disease 2019 (COVID-19); computed tomography (CT); ground-glass nodules; exudation lesions; imaging parameters

Submitted Apr 22, 2020. Accepted for publication Sep 11, 2020.
doi: 10.21037/qims-20-603
View this article at: http://dx.doi.org/10.21037/qims-20-603

Introduction

The coronavirus disease 2019 (COVID-19) pandemic has spread widely to many countries. Computed tomography (CT) plays a vital role in the diagnosis and follow-up of the disease (1). Advances in CT technologies have greatly improved the efficiency of clinical CT examinations. In China, about 220 million CT scans are performed each year (2). The diagnostic reference level of chest CT is 8 mSv, based on the Publication 102 of the International Commission on Radiological Protection (3), and the typical effective dose in China is 6.6 mSv (4), both significantly higher than the typical dose of chest digital radiography (0.02 mSv). Patients who undergo recurrent CT scanning are at higher risk of cancer due to radiation exposure (5), and COVID-19 patients often require multiple CT scans in a short period. Many factors affect radiation dose and image quality in CT scans, such as tube voltage, mAs, pitch, collimation, iterative algorithm level, and hardware and software. One of the ways to ensure radiological protection optimization is to set the scanning parameters according to the clinical purpose or the pathological features of the scanned body parts. For COVID-19, only the areas in the lungs need to be focused on, rather than the mediastinum. The lung is well inflated and provides high contrast to a mass or nodule, which can be detected easily, even when using lower-dose CT scanning. To the best of our knowledge, there is no gold standard routine scanning protocol, and the dose of lung CT can be reduced to some degree for the detection of lung ground-glass nodules and exudation lesions among COVID-19 patients.

This study aims to assess the influence of CT scanning parameters for detecting lung lesions and radiation dose and determine the threshold of scanning parameters to meet the requirements for image quality and lower radiation dose.

Methods

Patient selection and measurements

The images and clinical data of the COVID-19 inpatients at Beijing Ditan Hospital, Capital Medical University (China) were retrospectively analyzed. The diagnostic criteria and clinical subtypes were consistent with 'The diagnosis and treatment scheme of the novel coronavirus pneumonia (trial version 6)' (6). Thirty-two patients were enrolled and 11 patients specifically had mild COVID-19 and 21 patients had severe COVID-19. The mild COVID-19 patients were selected from March 17, 2020, to March 22, 2020. Inclusion criteria were as follows: (I) patients underwent chest CT examination at first admission; (II) time from onset to the first CT scan was <5 days. Lesion size and CT values in the relatively uniform and lowest-density areas in the CT images were measured. These measurements were used for the selection of simulated nodules with different densities in subsequent experiments. The purpose of measuring the CT values of low-density lesion areas was to provide the most challenging scenarios for detecting the simulated lesions with corresponding densities. The results from the mild cases were as follows: (I) lesion size >10 mm; and (II) CT values ranging from −727 to −230 HU.

The severe COVID-19 patients were selected from January 27, 2020, to March 21, 2020. They all underwent >1 recurrent CT scan. The CT values in the relatively flat area of lesions in recurrent CT images were measured. All severe COVID-19 cases presented a large range of diffuse exudative lesions, with CT values ranging from −80 to 0 HU.

The volume CT dose index (CTDIvol) values for all cases were recorded and averaged. The mean CTDIvol was 17 mGy for mild COVID-19 patients and 13.5 mGy for severe COVID-19 patients.

Phantom and simulated lesion selection

The anthropomorphic thorax phantom simulating an intermediate-sized adult (PH-1, Kyoto Kagaku, Kyoto, Japan), with 9 spherical nodules of different diameters (8, 10, and 12 mm in diameter) and CT values of −800, −630, and 100 HU at 120 kV, were used for the present study.

No patients were scanned in the study, and ethics approval was not required. Based on the lesion

Table 1 Distribution of 13 simulated lesions in the lungs

Lesions	12 mm	10 mm	8 mm	Custom
100 HU	Hilus of right lung	Hilus of left lung	Left upper lung	
–630 HU	Right chest wall of right lower lung	Anterior chest wall of right upper lung	Left costophrenic angle	
–800 HU	Left costophrenic angle	Anterior chest wall of left upper lung	Posterior chest wall of right lower lung, adjacent to spine	
Fat				Posterior chest wall of right lower lung; anterior chest wall of right upper lung
Ethanol				Middle lobe of right lung; middle lobe of left lung

measurements of the COVID-19 inpatients (all lesions >10 mm), the 3 sizes of simulated lesions (8, 10, and 12 mm in diameter) met the lesion size simulation requirements. The nominal CT value of the lowest-density nodules (–800 HU) was far lower than that of the pulmonary lesions among COVID-19 patients (lowest CT value: –727 HU). The CT detection requirements for simulated nodules were higher than those of lesions among COVID-19 patients. The 9 simulated lesions with different densities and diameters were placed in the cavity of the chest phantom according to the distribution features of COVID-19 lesions (7). At the same time, to simulate the exudative lesions (lowest at –80 HU) in critically ill patients, 4 custom-simulated lesions were also constructed, including 2 porcine fat pieces (–96 HU) and 2 capsules filled with 75% ethanol (–132 HU) with a diameter of about 2 cm. These were distributed in the lungs, as shown in *Table 1*.

Phantom scanning

All data acquisitions were performed on an 8-cm detector Philips Brilliance iCT scanner (Philips Healthcare, Cleveland, OH, USA). The phantom was scanned at 120, 100, and 80 kV separately using parameters from a routine chest CT scanning protocol, such as auto milliampere modulation (i.e., Doseright and 3-D modulation), 24 Doseright Index, 1.0 pitch, and 80-mm collimation. For every kilovolt, the phantom was scanned at milliampere-seconds (mAs) ranges from 10 to 100. The mAs were increased by 10 for each subsequent scan, whereas all other parameters remained unchanged. The scans were repeated for separate combinations of pitch (0.6, 0.8, 1.0, 1.15, and 1.49) and collimation (10, 20, 40, and 80 mm) at 80 kV and 100 mAs. The CTDIvol values were recorded for all the scans. Image data were measured and analyzed. Exposure parameters were confirmed at the threshold of meeting the diagnostic requirements of image quality. The Doseright Index settings were then adjusted so that the output radiation dose when scanning the phantom matched the threshold values. The anterior chest wall and lateral portions of the phantom were covered with the saline water bags (about 5-cm thickness) to simulate obese patients. Scanning was performed with the optimized conditions of the Doseright Index settings, and image quality was evaluated. In clinical practice, the CT scanner can automatically adjust the output dose according to the size of the patient to obtain stable image quality.

Image reconstruction and reformation

All scanning data were reconstructed to images with a standard lung algorithm, Y-sharp filter, 1-mm slice thickness and 1-mm interval, and iDose4 level 3. For 120-kV scans with 10–30 mAs, 100-kV scans with 10–50 mAs, and 80-kV scans with 10–50 mAs, the images were reconstructed with iDose4 levels 3–7. Axial and coronal images with 5-mm-slice thickness and 5-mm interval were reformatted.

Data measurement

Regions of interest (ROIs) were measured for all acquired images, including the right lower lung nodule of –800 HU adjacent to the spine, right lower lung nodule of –630 HU at the right chest wall, and left costophrenic angle nodules of –800 and –630 HU. These 4 nodules were located at regions more prone to COVID-19 lesions (*Figure 1*). The mean values and standard deviations were measured for 4 typical nodules, adjacent flat regions as background, fat, and ethanol-simulated lesions. Two senior radiographers performed all of the measurements. The 2 datasets

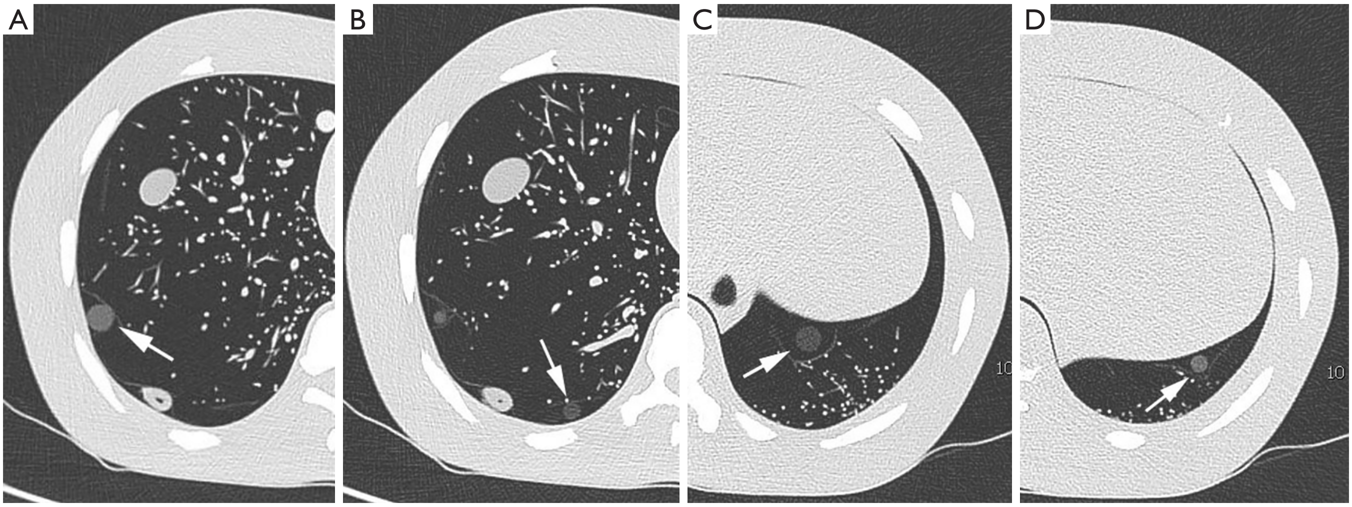

Figure 1 Four nodules with –630 HU (A, 12-mm diameter; D, 8-mm diameter) and –800 HU (B, 8-mm diameter; C, 12-mm diameter) were selected for measurements. The arrows indicate simulated nodules with different density and size.

were averaged and used to calculated contrast-to-noise ratio (CNR) and figure of merit (FOM) as the following formulas:

$$CNR = \frac{\left| H_{ROI} - H_{background} \right|}{\sqrt{\frac{\sigma_{ROI}^2 + \sigma_{background}^2}{2}}} \quad [1]$$

$$FOM = \frac{CNR^2}{CTDI_{vol}} \quad [2]$$

where σ is the standard deviation of the CT values in the ROI of the nodule or the adjacent flat region. HU is the mean CT value in the nodule ROI and the adjacent flat region.

Subjective evaluation

Two senior radiologists read and evaluated all images subjectively. They individually interpreted the visualization of all nodules and lesions in the lungs and recorded these if they could be detected. The overall image quality was rated on a 3-point Likert scale: 3 points represented very good quality (the texture displayed, the lesion boundary visible, low image noise, and fully meeting the diagnostic requirements); 2 points represented good quality (texture relatively clearly displayed, lesion boundary discernable, relatively high noise, and meeting the diagnostic requirements); and 1 point represented poor quality (unclear texture appearance, fuzzy lesion boundaries, large image noise, inadequately displaying ground-glass nodules). Image quality was considered unqualified if 1 of the radiologists could not observe the nodule or if the image noise was deemed too large to be accepted. If the lesion was faint in the image, details should be compared with those of surrounding tissues to determine whether the lesion could be identified. Only images of the lung tissue algorithm were presented for evaluation, and only lung lesions were considered for evaluation. The evaluation was conducted in accordance with the order of the CTDIvol and iDose level from low to high to avoid influence from a priori knowledge of lesion location from higher-dose images.

Statistical analysis

Statistical analysis was conducted with R software (version 3.5.2; http://www.r-project.org/). Repeated-measures analysis of variance was conducted to compare CNR and FOM among different scanning conditions. A kappa coefficient was calculated for assessing interobserver agreement; 0.00–0.40, 0.41–0.74, and 0.75–1.00 suggested poor, moderate, or good agreement, respectively. Two-sided $P<0.05$ indicated statistical significance.

Results

Influence of tube voltage and current on image quality

Statistical results showed that, at a fixed voltage of 120 or

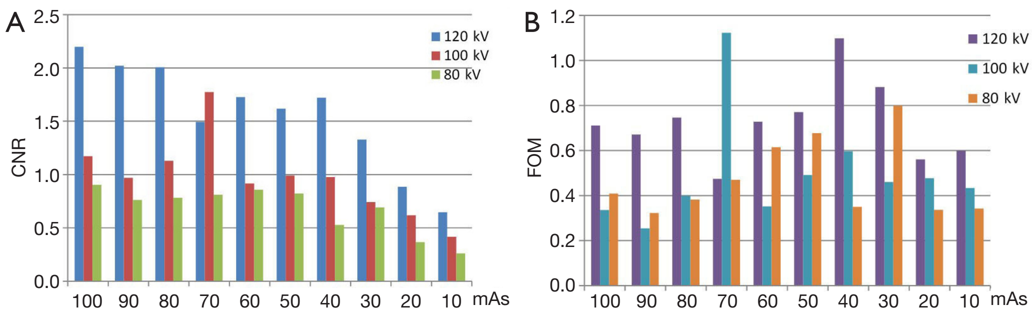

Figure 2 Contrast-to-noise (CNR) (A) and figure of merit (FOM) (B) of −800 HU nodule at the left costophrenic angle under different combinations of kilovolts and mAs.

Table 2 Subjective evaluation of axial and coronal images using different scanning parameters

Kilovolt	Scanning parameters		−800 HU nodule sizes			Radiologist A†				Radiologist B†			
						iDose4 level 3		iDose4 level 7		iDose4 level 3		iDose4 level 7	
	Milliampere-second	Volume CT dose index (mGy)	12 mm‡	10 mm‡	8 mm‡	Axial	Coronal	Axial	Coronal	Axial	Coronal	Axial	Coronal
120	10	0.7				2	2	3	3	1	2	2	3
100	30	1.2				2	3	3	3	1	3	2	3
	20	0.8				2	3	3	3	1	3	2	3
	10	0.4			345	1	2	2	2	1	2	2	2
80	70	1.4				2	3	3	3	1	3	2	3
	60	1.2				2	3	3	3	1	3	2	3
	50	1.0				2	3	3	3	1	3	2	3
	40	0.8				1	2	3	3	1	2	2	3
	30	0.6	3		334455	1	1	2	2	1	1	1	2
	20	0.4	3456		334455	1	2	2	2	1	1	1	2
	10	0.2	33445567	3345	3344556677	1	1	1	1	1	1	1	1

†, numbers 1–3 in the eight columns refer to rated image quality on a 3-point Likert scale: 3 points indicates very good quality and 1 point indicates poor image quality. ‡, numbers 3–7 in the 3 columns refer to iDose4 levels of 3–7. Location where the number appears in the table represents a −800 HU nodule of specific size that could not be identified in the image of this iDose4 level in that scanning parameter. Two same consecutive numbers indicate that the nodule in the image could not be detected by both radiologists.

100 kV, with increasing mAs, the image noise tended to decrease, and the CNR tended to increase (F=9.694 and P=0.033 for 120 kV; F=9.028 and P=0.034 for 100 kV). The FOM trend was the same as that of CNR (F=2.768 and P=0.174 for 120 kV; F=1.915 and P=0.255 for 100 kV). At 80 kV, the CNRs and FOMs had no significant change with increasing mAs (F=4.522 and P=0.114 for CNRs; F=1.212 and P=0.351 for FOMs) (*Figure 2*).

Using all kilovolt and milliampere-second combinations, all the simulated lesions, including porcine fat pieces and ethanol capsules, except the −800 HU nodules, were detected in the interpretation for 1-mm thickness images. *Table 2* shows the subjective evaluation results of the undetectable nodules and the unacceptable image quality. There were differences between the detection ability of nodules and the image quality of overall subjective evaluation among the radiologists. Using scanning parameter combinations, all the nodules could be detected by the radiologists; however, there were instances where image noise could not be subjectively accepted.

The scanning conditions are listed in *Table 2*. At least 1 radiologist believed that the image quality could not be interpreted. Radiologist B had slightly higher requirements on image quality than radiologist A (kappa coefficient: 0.467, moderately consistent). The image quality of iDose4 level 7 was generally higher than that of level 3.

Effect of pitch on image quality

Both nodules of −630 HU showed higher CNR in the range of 0.6–1.49 (*Figure 3*). For the 2 nodules of −800 and −630 HU, CNRs had no statistical differences at each of the 5 pitches (F=0.673, P=0.476). Based on these findings, it is recommended that a pitch be used is not >1. There was no change in the image quality scores with different pitches among the 2 radiologists.

Effect on image quality of collimation (detector array width)

At 80 kV and 100 mAs, and other parameters remaining consistent, the radiation dose varied greatly with different detector array widths. However, for each of the nodules, the CNRs and FOMs at each of the 4 collimations had no statistical differences (F=2.509 and P=0.125 for CNRs; F=1.485 and P=0.309 for FOMs) (*Figure 4*). The CTDIvol was 2.9 mGy at 10-mm collimation and 2 mGy with a 31% reduction at 80-mm collimation. Therefore, it is recommended to use a wider detector array for lung CT. Image quality grading was consistent between the 2 radiologists for different collimations.

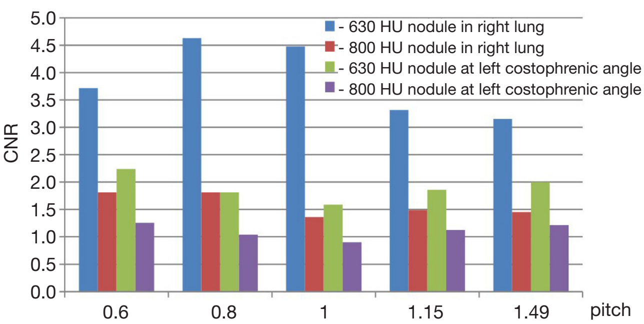

Figure 3 Contrast-to-noise ratio (CNR) values of 4 nodules in the lung with different pitches.

Effect of iterative reconstruction algorithm on image quality

CNR values and subjective evaluation scores increased with increasing parameter values for each imaging iteration (*Figure 5*). The number of qualified images also increased. The quality of many images did not meet diagnostic requirements at iDose4 level 3 but was satisfied at level 7 (*Table 2*). At the same time, the ratio of qualified images to unqualified images was also improved when combined with the axial and coronal slices with the 5-mm thickness (*Figure 6*).

Image quality at the threshold of scanning conditions

The CNR and FOM values of the nodules in the qualified images at the threshold of scanning parameters are shown in *Table 3*. At 3 parameter combinations (120 kV/20 mAs, 100 kV/40 mAs, and 80 kV/80 mAs), the CNRs of 4 nodules were found to be statistically different (P=0.038), but the FOMs had no statistical differences (P=0.085) (*Figure 7*). As seen in the *Table 3*, under the 3 threshold conditions, the CNR and FOM values of the 4 nodules were highest at 100 kV and 40 mAs. There were differences

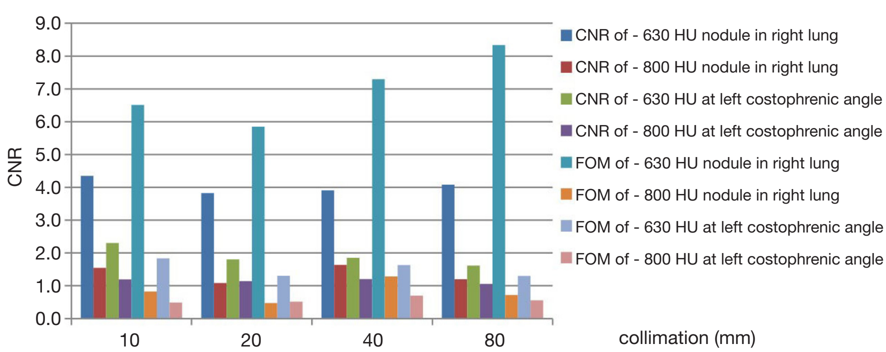

Figure 4 Contrast-to-noise ratio (CNR) and figure of merit values (FOM) of the nodules in the lung with different collimations at 80 kV and 100 mAs.

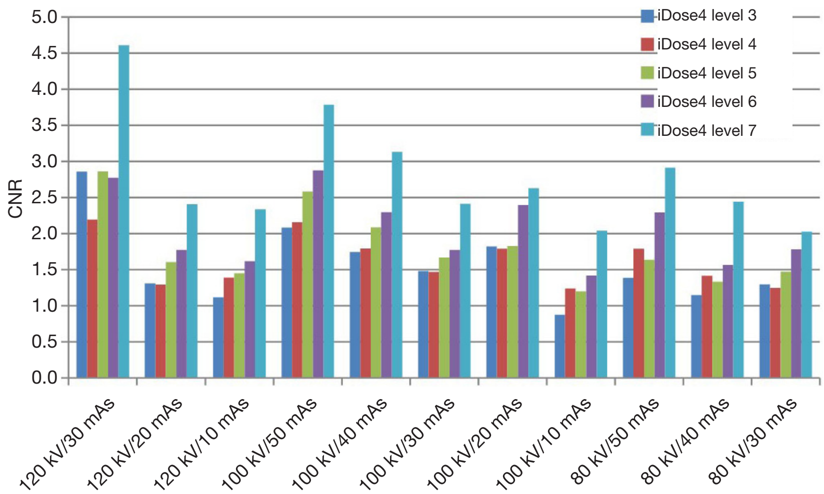

Figure 5 Contrast-to-noise (CNR) values of lung nodules with different iterative reconstruction levels.

between the tolerance of subjective perception to image quality and the ability to detect nodules. The tolerance of subjective perception to image quality was an important factor in increasing radiation dose.

Comparison of conventional and optimized scanning protocols

Using the conventional scanning protocol, the radiation doses of phantom scanning at different kilovolts are shown in *Table 4*. According to the critical scanning parameters obtained in the experiments, Doseright Index set values, and corresponding dose values are shown. The Doseright Indexes were used to scan simulated obese patients. The radiation doses were increased accordingly, and the resulted image quality met the diagnostic requirements.

Discussion

When using chest CT for COVID-19 patients for exudation or nodules in the lungs, it is vital to consider its justification and to minimize false negatives (8,9). The difference between CT values of nodules and the lung field is great, which provides the possibility of reducing the radiation dose (10). The measurement results of the present study showed that the CT value of COVID-19 lesions was lowest at −727 HU, which was relatively easy to detect. Low CT value nodules in some regions are difficult to detect, such as the costophrenic angles, which are adjacent to the transverse septum and abdominal organs with higher density, resulting in large noise areas, thereby reducing the detectability of lesions in these areas. Another area of difficulty is the posterior chest wall region beside the spine. At lower tube potentials, the artifact of X-ray beam hardening is more significant, which harms depicting nearby structures. The low CT value-simulated nodules were placed in these regions in the present study for these reasons.

Multiple chest CT scans are required for COVID-19 patients in a short period. Several strategies and technologies can help users to reduce and optimize the radiation dose associated with CT scans (11,12). The reduction of tube current and tube potential are the mainstays of dose-reduction methods (13). Tube potential reduction often requires higher tube current for satisfactory image quality, but may still contribute to significant radiation dose reduction. The goal of the present study was to determine whether the optimal combination of kilovolt and mAs could meet the diagnostic requirements and minimize radiation dose for chest imaging. The results showed that lesions with CT values >−630 HU could be detected under all scanning conditions, which indicated that the requirement of dose level for pulmonary nodules was not high. For recurrent CT scans among severe COVID-19 patients, in particular, diffuse exudative lesions were found in the lung, and CT values were >−80 HU, indicating low demand for image quality. The findings of the present study also showed that the simulated lesions of porcine fat pieces and ethanol capsules were detectable at all scanning conditions. Therefore, the radiation dose could

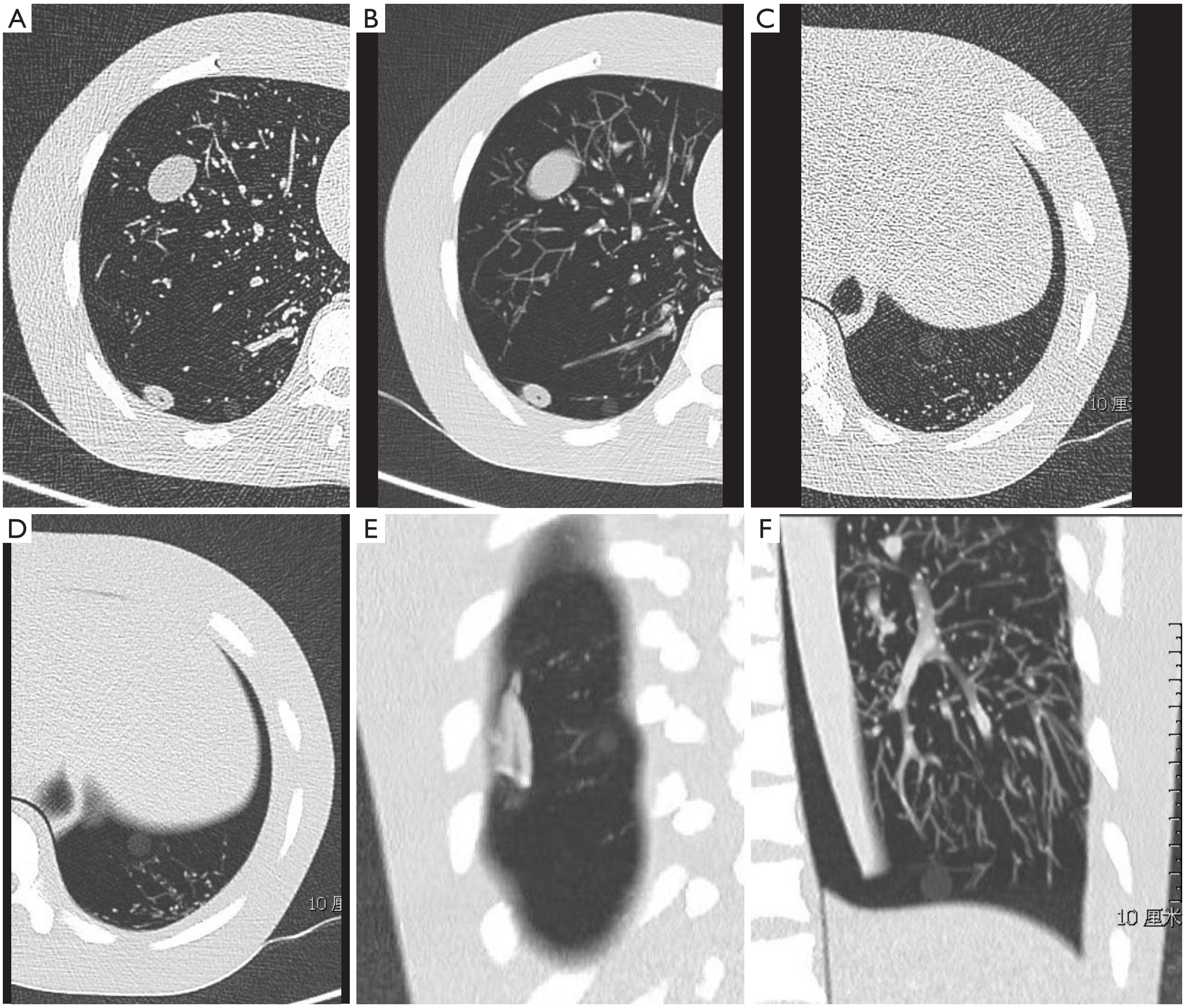

Figure 6 Two nodules of –800 HU in the lung with 1-mm (A,C) and 5-mm (B,D with axial; E,F with coronal) thickness at 80 kV and 40 mAs.

Table 3 Contrast-to-noise (CNR) and figure of merit (FOM) values of different nodules at the threshold of scanning conditions

Kilovolt	Tolerance threshold of subjective perception to image quality											Image quality threshold of –800 HU nodules observed									
	Milliampere-second	Volume CT dose index (mGy)	CNR				FOM				Milliampere-second	Volume CT dose index (mGy)	CNR				FOM			
			A	B	C	D	A	B	C	D			A	B	C	D	A	B	C	D
120	20	1.4	2.7	1.2	1.4	0.9	5.0	1.0	1.4	0.6	10	0.7	1.9	0.9	1.2	0.6	5.2	1.2	2.3	0.6
100	40	1.6	3.1	1.6	1.7	1.0	6.1	1.7	1.8	0.6	20	0.8	2.5	1.0	1.5	0.6	7.9	1.1	2.7	0.5
80	80	1.6	3.0	1.4	1.0	0.8	5.7	1.3	0.6	0.4	40	0.8	2.4	1.1	1.2	0.5	7.5	1.4	1.8	0.4

A, –630 HU nodule with 12-mm diameter at right chest wall of right lower lung; B, –800 HU nodule with 8-mm diameter at posterior chest wall of right lower lung, adjacent to spine; C, –630 HU nodule with 8-mm diameter at left costophrenic angle; D, –800 HU nodule with 12-mm diameter at left costophrenic angle.

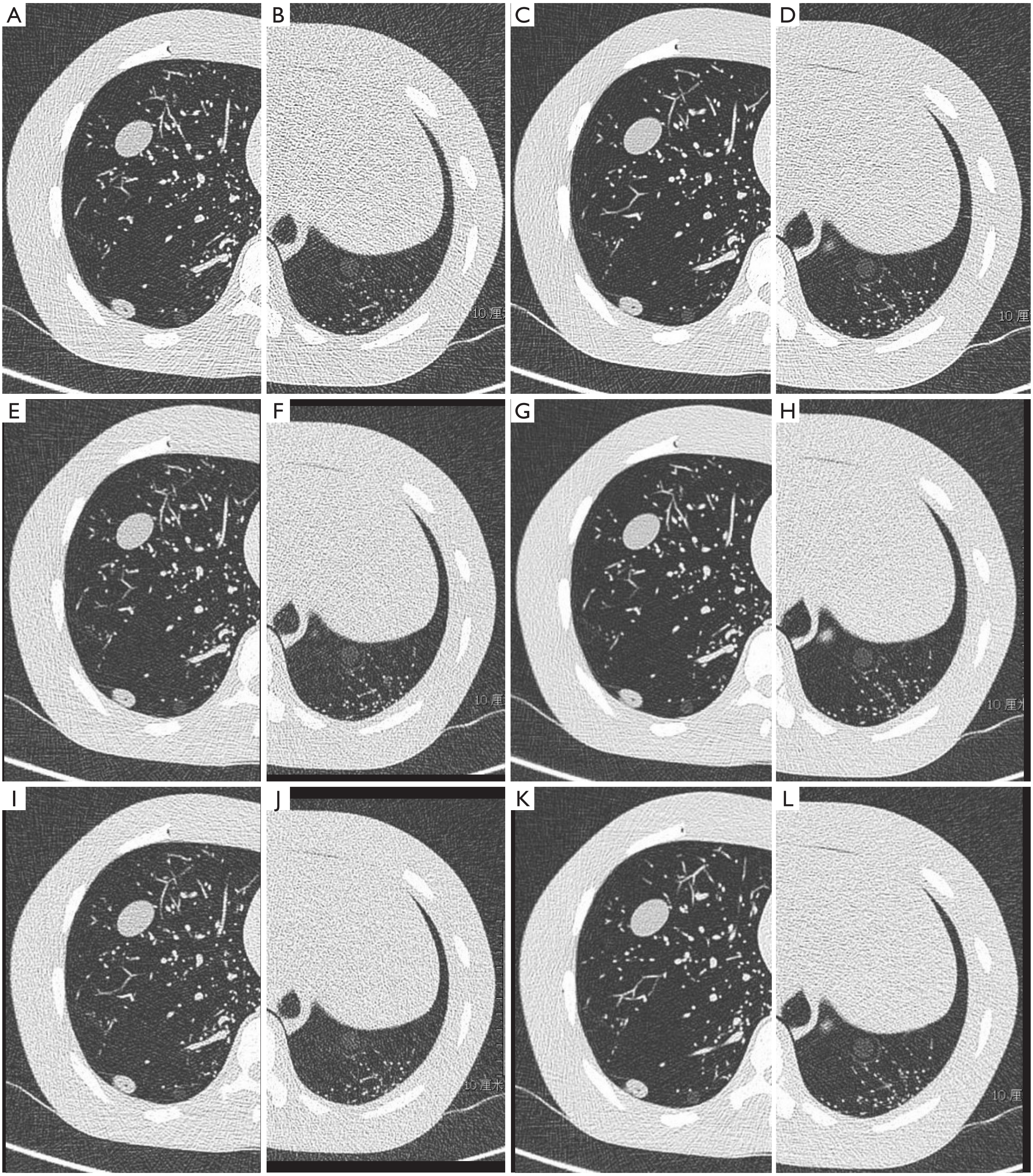

Figure 7 Nodules of –800 HU with 1-mm thickness acquired at 6 types of scanning conditions. (A,B) 120 kV and 10 mAs; (C,D) 120 kV and 20 mAs; (E,F)100 kV and 20 mAs; (G,H) 100 kV and 40 mAs; (I,J) 80 kV and 40 mAs; (K,L) 80 kV and 80 mAs.

Table 4 Radiation doses of the phantom with scanning parameters before and after optimization

Kilovolt	Conventional scanning parameters			Scanning parameters after optimization			Doses for obese patients after optimization	
	Doseright index	Milliampere-second	Volume CT dose index (mGy)	Doseright index	Milliampere-second	CTDIvol (mGy)	Milliampere-second	Volume CT dose index (mGy)
120	24	208	14.1	1	22	1.5	28	1.9
100	24	299	12.1	2	41	1.7	54	2.2
80	24	871	17.0	3	87	1.7	130	2.6

theoretically be reduced to the lowest level allowed by the CT equipment (14). The density of −800 HU nodules was similar to that of COVID-19 in the initial appearance of intrapulmonary exudation. The detectable rate was affected by the increase of noise caused by low radiation dose. It was necessary to adopt a conservative attitude and increase the radiation dose appropriately to reduce the probability of a missed diagnosis.

In clinical practice, the acceptability of image quality, especially image noise, varies among radiologists. The excessive pursuit of low noise images will not result in more diagnostic information but will lead to an increase in unnecessary radiation dose because of a lack of diagnostic confidence. In the design of the present study, to not overlook COVID-19 exudative or nodular lesions, even if the simulated lesions could be detected, we judged that they did not meet diagnostic requirements if the overall image quality could not be accepted subjectively by 1 of the radiologists. The density of −800 HU nodules was far lower than that of mild COVID-19 lesions in the present study. If the −800 HU nodules could be shown in the image, the COVID-19 lesions must also be detectable. Ideally, the physician's acceptability of the overall quality of the image should be consistent with the detective limitation of the lowest-density nodules, so that the optimization of scanning parameters is truly achieved.

Theoretically, image quality increases at lower pitches. The data in the present study indicate that a lower pitch is appropriate for nodules, especially for ground-glass nodules. However, when considering increases in scanning time, it is recommended that the pitches selected are not >1.

The popularity of iterative reconstruction algorithms has led to a dramatic reduction in image noise and radiation dose (15-17). In the present study, when iDose4 level 7 was used, the proportion of the obtained images meeting the diagnostic requirements greatly increased. Iterative model reconstruction (IMR) might be able to broaden the experiment results further, although there are different results and opinions (18,19). At the same time, although the thin slices showed details in high resolution, the significant increase in noise harmed the appearance of the ground-glass nodule boundary. For the early faint exudative lesions of COVID-19, the focus is on whether they can be detected. Higher-contrast resolution is not required. The results of the present study showed that using a higher-slice thickness (i.e., 5 mm) could effectively reduce noise and improve ground-glass nodule appearance. Combined with the reformatted coronal or sagittal images, the transmission capability of image information could be greatly improved. Partial volume effect might cause the thicker slices to miss the tiny nodules, so it is recommended that an appropriate slice thickness is used to display the image information continuously on the diagnostic workstation in clinical practice.

The results of the present study showed that, for patients with regular body size, the optimal conditions were 100 kV, 40 mAs, or the corresponding automatic current modulation setting. For larger patients, 120 kV could be used to improve beam penetration, and 20 mAs or the corresponding automatic current setting. If the patient is very small size or a child, 80 kV, and the corresponding parameter setting could be used. The Doseright Index levels set according to the experimental results could generate satisfactory image quality for obese patients.

The present study has several limitations. First, the attenuation capacity of the phantom was slightly less than that of typical adults, but the relationship between the imaging parameters reflected in the experiments and the image quality could be observed. The thresholds of the scanning conditions were fed back to the Doseright Index setting, which avoided the deficiencies caused by the phantom. Second, we did not discuss the influence of chest CT image quality and radiation dose of new iterative algorithms (IMR), nor did we provide a comparison with iDose4 and other reconstruction techniques. Third, we did not include noise simulation in the raw data domain in the real standard-dose scans. The influence of parameter changes, such as kilovolts, collimation, and pitch on breast dose was not included, and further consideration will be given to this in future research.

The important role of CT in the worldwide epidemic of COVID-19 is unquestionable. For the detection of lung ground-glass nodules and exudation lesions, the dose of chest CT can be reduced to a very low level of 1.6 mGy at 100 kV/40 mAs for standard patients. It is the responsibility of medical personnel to minimize the radiation dose to patients to reduce the risk of exposure.

Acknowledgments

Funding: None.

Footnote

Conflicts of Interest: All authors have completed the ICMJE uniform disclosure form (available at http://dx.doi.org/10.21037/qims-20-603). The authors have no conflicts of interest to declare.

Ethical Statement: No patients were scanned in the study, and ethics approval was not required.

References

1. Deng ZQ, Zhang XC, Li YR, Xu HB, Gang YD, Wang HL, Liao RF, Jin YH, Wang XH, Zeng XT, Luo SH, Pan ZY. Value of chest CT screening in the early COVID-19 outbreak. Chin J Radiol 2020;54:430-34.
2. Niu YT, Su YP, Liang J, Hou CS, Sun QF. Study on estimation of medical exposure frequency in China. Chin J Radio Med Prot 2019;29:325-30.
3. Valentin J; International Commission on Radiation Protection. Managing patient dose in multi-detector computed tomography(MDCT). ICRP Publication 102. Ann ICRP 2007;37:1-79, iii.
4. Ministry of Health of the People's Republic of China. WS/T 637-2018 Diagnostic reference levels for adults in X-ray computed tomography. Beijing: Standards Press of China, 2018.
5. Sodickson A, Baeyens PF, Andriole KP, Prevedello LM, Nawfel RD, Hanson R, Khorasani R. Recurrent CT, cumulative radiation exposure, and associated radiation-induced cancer risks from CT of adults. Radiology 2009;251:175-84.
6. National Health Commission of the People's Republic of China. The diagnosis and treatment scheme of the novel coronavirus pneumonia (trial 6th trial version) [EB/OL]. (2020-02-18) (2020-02-19). Available online: http://www.nhc.gov.cn/yzygj/s7653p/202002/8334a8326dd94d329df351d7da8aefc2.shtml
7. Du S, Gao S, Huang G, Li S, Chong W, Jia Z, Hou G, Wáng YXJ, Zhang L. Chest lesion CT radiological features and quantitative analysis in RT-PCR turned negative and clinical symptoms resolved COVID-19 patients. Quant Imaging Med Surg 2020;10:1307-17.
8. Liu WH, Wang XW, Cai ZQ, Wang X, Huang XL, Jin ZG. Chest CT as a screening tool for COVID-19 in unrelated patients and asymptomatic subjects without contact history is unjustified. Quant Imaging Med Surg 2020;10:876-7.
9. Chan LL, Tan EK. Chest CT in asymptomatic COVID-19: benefits and concerns. Quant Imaging Med Surg 2020;10:1570-1.
10. Agostini A, Floridi C, Borgheresi A, Badaloni M, Esposto Pirani P, Terilli F, Ottaviani L, Giovagnoni A. Proposal of a low-dose, long-pitch, dual-source chest CT protocol on third-generation dual-source CT using a tin filter for spectral shaping at 100 kVp for CoronaVirus Disease 2019 (COVID-19) patients: a feasibility study. Radiol Med 2020;125:365-73.
11. Liu DD, Niu YT. Effects of different scout images on radiation dose in CT scanning using automatic tube current modulation. Chin J Radiol 2017;51:525-8.
12. Singh S, Kalra MK, Ali Khawaja RD, Padole A, Pourjabbar S, Lira D, Shepard JA, Digumarthy SR. Radiation dose optimization and thoracic computed tomography. Radiol Clin North Am 2014;52:1-15.
13. Kubo T, Ohno Y, Kauczor HU, Hatabu H. Radiation dose reduction in chest CT--review of available options. Eur J Radiol 2014;83:1953-61.
14. Gordic S, Morsbach F, Schmidt B, Allmendinger T, Flohr T, Husarik D, Baumueller S, Raupach R, Stolzmann

P, Leschka S, Frauenfelder T, Alkadhi H. Ultralow-dose chest computed tomography for pulmonary nodule detection: first performance evaluation of single energy scanning with spectral shaping. Invest Radiol 2014;49:465-73.

15. Howard SA, Rosenthal MH, Qin L, Matalon SA, Bernard BD, Beard CJ, Sweeney CJ. Quantifying Decreased Radiation Exposure From Modern CT Scan Technology and Surveillance Programs of Germ Cell Tumors. Am J Clin Oncol 2018;41:949-52.
16. Afadzi M, Lysvik EK, Andersen HK, Martinsen ACT. Ultra-low dose chest computed tomography: Effect of iterative reconstruction levels on image quality. Eur J Radiol 2019;114:62-8.
17. Lim HK, Ha HI, Hwang HJ, Lee K. High-pitch, 120 kVp/30 mAs, low-dose dual-source chest CT with iterative reconstruction: Prospective evaluation of radiation dose reduction and image quality compared with those of standard-pitch low-dose chest CT in healthy adult volunteers. PLoS One 2019;14:e0211097.
18. Kim H, Park CM, Song YS, Lee SM, Goo JM. Influence of radiation dose and iterative reconstruction algorithms for measurement accuracy and reproducibility of pulmonary nodule volumetry: A phantom study. Eur J Radiol 2014;83:848-57.
19. Sung P, Lee JM, Joo I, Lee S, Kim TH, Ganeshan B. Evaluation of the Impact of Iterative Reconstruction Algorithms on Computed Tomography Texture Features of the Liver Parenchyma Using the Filtration-Histogram Method. Korean J Radiol 2019;20:558-68.

Cite this article as: Niu Y, Huang S, Zhang H, Li S, Li X, Lv Z, Yan S, Fan W, Zhai Y, Wong E, Wang K, Zhang Z, Chen B, Xie R, Xian J. Optimization of imaging parameters in chest CT for COVID-19 patients: an experimental phantom study. Quant Imaging Med Surg 2021;11(1):380-391. doi: 10.21037/qims-20-603